Materials Today Energy 56 (2026) 102197

Contents lists available at ScienceDirect

Materials Today Energy

journal homepage: www.journals.elsevier.com/materials-today-energy/

Improved environmental stability of perovskite films enabled by a one-pot synthesized eco-friendly additive

Miguel Guerrero [a], Jesús Sanchez-Diaz [b], Gabriela S. Anaya-González [a], Oscar González-Antonio [a], Lorena Martínez-dlCruz [a], Margarita Romero-Ávila [a], Rosa Santillan [c], Iván Mora-Seró [b], Jesús Rodríguez-Romero [a,*]

[a] Facultad de Química. Universidad Nacional Autónoma de México., Ciudad Universitaria, 04510, Ciudad de México, Mexico
[b] Institute of Advanced Materials (INAM), Universitat Jaume I, 12006, Castelló, Spain
[c] Departamento de Química, Centro de Investigación y de Estudios Avanzados del IPN, 07000, Apdo, 14-740, Ciudad de México, Mexico

A B S T R A C T

The long-term instability of metal halide perovskites, such as $MAPbI_3$ and $FAPbI_3$, remains a major obstacle to their commercialization. This study introduces a multifunctional-organic-additive (agent 1), synthesized via a one-pot reaction using ethanol as a green solvent, offering an environmentally benign approach. Agent 1 was incorporated into $MAPbI_3$ films through antisolvent treatment and surface passivation, enhancing both shelf and operational stability. Under moderate humidity (35–45 %), antisolvent-treated films showed only 23 % degradation after ~36 days, compared to 60 % in untreated samples. At higher humidity (55–65 %), passivated films retained 67 % of the original material, while reference films degraded by 97 %. On the other hand, solar cells treated with agent 1 maintained 91 % of their initial efficiency after 60 min of continuous operation. Long-term storage tests (168 h) revealed a 41 % efficiency drop in reference devices, versus 13 % and 29 % in antisolvent- and passivated-treated devices, respectively. Agent 1 also exhibited excellent thermal/chemical stability, with negligible decomposition above 200 °C and only 0.35 % weight loss after 24 h at 95 °C. Its molecular integrity was confirmed via ^{1}H NMR after one year. Combining ease of synthesis, environmental safety, and multifunctionality, agent 1 is a promising candidate for industrial-scale stabilization of perovskite solar cells.

1. Introduction

Despite remarkable progress in the power conversion efficiency of perovskite-based photovoltaic devices, their limited operational and environmental stability remains a critical bottleneck for commercialization. External stressors such as moisture [1], oxidizing agents [2], and thermal fluctuations [3] accelerate structural and functional degradation, severely compromising device performance and longevity. A promising strategy to mitigate these issues involves the incorporation of molecular additives [4]. These compounds have demonstrated the ability to enhance crystallinity [5,6], passivate structural defects [7], and improve environmental stability, particularly against moisture-induced degradation [8,9]. Among several kinds of defects, halide vacancies are especially detrimental, as they facilitate the escape of halogen anions in their molecular form (X_2) [10], a degradation pathway notably prevalent, for example, in $MAPbI_3$ perovskites [11]. To address this challenge, both organic (e.g., monomers, polymers, solvents) [12–14] and inorganic [15] materials have been explored, yielding encouraging results. Organic additives often feature functional groups such as carboxylic acid/carboxylate (–COOH/–COO^-) [16], carbonyl (–C=O) [17,18], thiocarbonyl (–C=S) [19], alcohol (–OH) [20], amino (–NH_2) [21], nitrile (–C ≡ N) [22], and halogen substituents (I, Br, Cl, F) [7,8]. These groups contain heteroatoms with lone electron pairs (e.g., N, O, S), which act as Lewis bases to fill halide vacancies and stabilize the perovskite lattice [23–26]. While organic molecules offer synthetic versatility and tunable functionality, their application introduces two key limitations: 1. Simple molecules, often organic salts, tend to be highly hydrophilic or possess low melting points, undermining long-term device stability [27]; and 2. Complex macromolecules or polymers typically require elaborate and costly synthetic routes [12, 28], restricting their accessibility to specialized laboratories. In this work, we present a novel organic additive designed to overcome these limitations, offering enhanced stability, defect passivation, and processability for $MAPbI_3$-based perovskite films and complete solar cell devices. Directing our attention towards durability, with simple molecules, we make a first approximation of a family, 4H-chromenes, of highly modifiable molecules, which makes them a range of possibilities to improve photovoltaic devices.

* Corresponding author.
E-mail address: jrr@quimica.unam.mx (J. Rodríguez-Romero).

https://doi.org/10.1016/j.mtener.2026.102197
Received 28 August 2025; Received in revised form 25 December 2025; Accepted 3 January 2026
Available online 4 January 2026

2. Experimental section

2.1. Materials and characterization

Benzaldehyde (Reagent Plus®, ≥99 %), 5,5-Dimethyl-1,3-Cyclohexanedione (≥99 %), Malononitrile (≥99 %) were purchased from Sigma-Aldrich. Lead Iodide (PbI_2, 99.99 %) was purchased from TCI. Methylammonium Iodide (MAI, 99.9 %) was purchased from Greatcell solar company. Tin Oxide (SnO_2, 15 % in H_2O) was purchased from Alfa Aesar. 2,20,7,70-tetrakis[N,N-di(4-methoxyphenyl)amino]-9,90-spirobifluorene (Spiro-MeOTAD, 99 %) was purchased from Feiming chemical limited. 4-tert-butylpyridine (tBP, 98 %), Bis(trifluoromethane) sulfonamide lithium salt (Li-TFSI, 99.95 %), Acetonitrile (ACN, 99.5 %), Chlorobenzene (CBz, 99.8 %), N,N-dimethylformamide (DMF, 99.8 %) and dimethylsulfoxide (DMSO, 99.8 %) were purchased from Sigma-Aldrich. All reagents were used without further purification.

2.2. Synthesis of 2-amino-5-oxo-4-phenyl-5,6,7,8-tetrahydro-4H-chromene-3-carbonitrile (agent 1)

100 mg of 5,5-dimethylcyclohexane-1,3-dione (0.714 mmol), 47 mg of malononitrile (0.714 mmol), and 96 μL of benzaldehyde (75 mg, 0.714 mmol) were placed in a flask and dissolved in 2 mL of absolute ethanol. Then, 7 μL of 10 % molar piperidine (6.08 mg, 0.0714 mmol) were added. A crystalline white powder was obtained with a yield of 95 % (199 mg; 0.676 mmol). The melting point was 202–204 °C. ^{1}H NMR spectra (600 MHz, DMSO-d6) showed signals at δ 7.28–7.26 (t, 2H), 7.18–7.12 (m, 3H), 6.99 (s, 2H), 4.16 (s, 1H), 2.25–2.23 (d, 1H), 2.11–2.08 (d, 1H), 1.03 (s, 3H), 0.94 (s, 3H). While ^{13}C NMR spectra (151 MHz, DMSO-d6) displayed signals at δ 195.67, 162.51, 158.50, 144.77, 128.35, 127.16, 126.58, 119.75, 112.74, 58.30, 49.98, 39.52, 35.58, 31.82, 28.41, 26.81.

2.3. Device fabrication

2.5 × 2.5 cm pre-patterned ITO substrates were washed in subsequent ultrasonic baths for 15 min each with water and soap, ethanol, acetone and isopropanol and finally dried with N_2 flow. Before the ETL deposition, a 20 min UV-Ozone treatment was performed, then a 3 w.t.% solution of SnO_2 was prepared by dissolving the 15 w.t.% stock solution with miliQ-water. Then it was deposited by spin-coating on top of the Glass/ITO substrate at 3500 rpm for 40 s, then it was annealed at 150 °C for 30 min. After the annealing and when the substrates cooled down, a 15 min UV-Ozone was performed before the perovskite deposition. A 1.24 M precursor solution was prepared by mixing 622 mg of PbI_2 and 215 mg of MAI and dissolved in 1 mL of DMF +0.095 mL of DMSO. Then the precursor solution was spin-coated on top of the SnO_2 layer at 4000 rpm for 20 s, then at the second ~6, 250 μL of CBz with (1 mg/ml of agent 1 in CBz) or without agent 1 was dropped in the center of the spinning substrate. After the spinning was finished, the substrate was annealed at 100 °C. for 10 min. For the passivated films, a 1 mg/ml of agent 1 in CBz solution was spin coated on top of the already formed perovskite film at 4000 rpm for 30 s dynamically and then annealed at 100 °C for 10 min. When the substrates were cooled down, the HTM was prepared dissolving 72.3 mg of spiro-OMeTAD, 28.8 μL of 4-tert-butylpyridine, and 17.5 μL of a stock solution of 520 mg/mL lithium bis-(trifluoromethylsulfonyl)imide in acetonitrile in 1 mL of chlorobenzene. Finally, 100 nm of gold was thermally evaporated. The films and complete devices were fabricated under ambient atmosphere, and once prepared, all analyses were carried out in air.

2.4. Preparation of thin films for pXRD analysis

2.5 × 2.5 cm pre-patterned FTO substrates were washed in subsequent ultrasonic baths for 15 min each with water and soap, ethanol, acetone and isopropanol and finally dried with N_2 flow. After drying, the cleaned substrates were subjected to a surface activation treatment consisting of UV/ozone exposure at 100 °C for 20 min using a SETCAS LLC Ozone Cleaner UV (Model SC-UV-1).

Perovskite thin films were deposited using a spin-coating process performed with an Ossila Spin Coater, programmed at 4000 rpm for 50 s. The perovskite precursor solution was prepared by dissolving 622 mg of lead iodide (PbI_2) and 215 mg of methylammonium iodide (MAI) in a solvent mixture of 1 mL N,N-dimethylformamide (DMF) and 0.095 mL dimethyl sulfoxide (DMSO), depositing an aliquot of 50 μL and 250 μL of CBz as an antisolvent at 3 s, ending with an annealing process at 100 °C for 10 min. For the incorporation of agent 1 as an additive, a 1 mg/mL solution in CBz was prepared and applied 250 μL during the antisolvent step after 3 s of starting the program it spins. In addition, a second batch corresponding to the passivating layer method was prepared, in which the additive was added 250 μL in a concentration of 1 mg/mL of CBz solution in a spin program identical to the one already mentioned, using a previously formed perovskite film, closing with a final annealing process at 100 °C for 10 min.

2.5. Thermal analysis

For TGA, initial temperature: 25 °C, final temperature: 250 °C. Heating rate: 2.5 °C min^{-1} under air. For isotherm, initial temperature: 20 °C, final temperature: 95 °C. Heating rate: 2.5 °C min^{-1} under air. The sample was then kept at that temperature for 24 h.

2.6. Films characterization

The XRD pattern of the prepared films were measured using X-ray diffractometer (D8 Advance DAVINCI, Bruker-AXS) (Cu Kα, wavelength λ = 1.5406 Å) within the range of 3–60°, step of 0.02° and counting time of 3 s per step.

2.7. Device characterization

J-V curves were measured using an Abet technologies (Sun 2000) solar simulator. The light intensity was adjusted to 1 sun (100 mW/cm^2) using a calibrated Si solar cell and a photodiode. The devices were measured in ambient conditions without encapsulation; the active area was defined by a mask which was 0.121 cm^2. The Shelf-stability measurements were measured using the same system.

MPP measurements were carried out in ambient conditions (T~60 °C and RH ≥ 45 %) using an Ossila solar simulator class AAA and automated J-V measurement system (T2003B3-G2009A1). The light intensity was adjusted to 1 sun (100 mW/cm^2) using a calibrated Si solar cell. The devices were not encapsulated.

2.8. Nuclear magnetic resonance of agent 1 and $MAPbI_3$ precursors

All results were measured on a 14.09 T (600 MHz) NMR Spectrometer Jeol brand, Model ECZ600R. For ^{1}H NMR, 2 different solutions were prepared; **a.** Contains 20 mg of Agent 1 and **b.** It contains 10 mg of Agent 1 + 14 mg of PbI_2 and 5 mg of MAI. For ^{13}C NMR, 2 different solutions were prepared; **a.** Contains 50 mg of Agent 1 and **b.** Contains 50 mg of Agent 1 + 70 mg of PbI_2 + 25 mg of MAI. All of this is measured in DMSO-D6.

2.9. IR studies

2.9.1. Thin films

For the preparation of these thin films, the same method described for pXRD was followed, in which it was differentiated by taking 250 μL from the original solution, to which 10 mg of Agent 1 was added and with this a new precursor solution was obtained. Thin films of $MAPbI_3$ and $MAPbI_3$ + Agent 1 were obtained. Both films were measured using a PerkinElmer Spectrum 400 FTIR/FIR spectrophotometer range: 4000 -

400 cm-^{1} with spectral resolution: 0.4–64 cm^{-1}.

2.9.2. Solution

For the measurement of the Fourier transform Infrared spectroscopy (FTIR) in solution, using a PerkinElmer Spectrum 400 FTIR/FIR spectrophotometer range: 4000 - 400 cm-^{1} with spectral resolution: 0.4–64 cm^{-1}. 4 different samples were prepared, corresponding to pure **1.** (DMSO), **2.** (DMSO + PbI_2), **3.** (DMSO + Agent 1) and finally **4.** (DMSO + PbI_2 + Agent 1). Each sample was prepared using 250 μL of DMSO, 14 mg of PbI_2, and 10 mg of Agent 1.

2.10. UV–Vis studies of extracted thin films

UV–Vis absorption spectra were obtained using a Thermo ScientificEvolution 220 dual beam spectrophotometer. Each measurement was made in a wavelength range of 700-270 nm with a spacing of 0.5 nm. Each sample was obtained by performing an extraction of formed films, control film (aged) and film with 10 mg of Agent 1 (aged). In the case of control films (fresh), antisolvent (fresh) and passivating layer (fresh), a triplicate was performed. In each extraction, 10 mL of toluene was used to fully submerge the film, which was then allowed to stand for 15 min at room temperature. From each undiluted extract, a volume of 3 mL was collected for analysis.

3. Results and discussion

To explore the potential of 4*H*-chromenes (4HC) as functional additives, we carried out the synthesis using a simple and versatile protocol. This procedure involves three key reactants: a diketone (e.g., 1,3-cyclohexanedione), an aldehyde with positions amenable to functionalization, and a molecule bearing a highly acidic α-hydrogen, such as malononitrile, Fig. 1a. The reaction can be performed under either acidic or basic catalysis [29,30], using a two-step or one-pot synthesis [31]. The resulting family of compounds naturally contains functional groups such as carbonyl, ether, amino, and nitrile, which are known to passivate halide vacancies [4,7]. Notably, the diketone and aldehyde structures can be modified to introduce additional functionalities (red, blue and green substituent in the scheme of the reaction). Therefore, there are extensive and varied possibilities for improving performance through molecular engineering.

Agent 1 was synthesized via a multicomponent reaction by combining all reactants in a single vessel, using ethanol as the solvent, Fig. 1a. Although alternative solvents such as water [32] and solvent-free conditions [33] have been reported in the literature under specific catalytic systems. In this study, ethanol was selected as solvent, due to its environmentally benign nature and its ability to deliver high yields when using simple catalysts like piperidine [31]. Upon stirring, the formation of a white precipitate was observed within minutes. Anyway, the reaction was allowed to proceed for 30 min at room temperature to ensure complete product formation. The resulting white powder was isolated by vacuum filtration, though gravity filtration was found to be equally viable, and washed with cold ethanol until the faint orange hue disappeared completely. This color change corresponds to the formation of a stable dissolved intermediate, arising from the interaction of the aldehyde and malononitrile precursors [34,35]. The reaction showed a yield of more than 95 %, highlighting its remarkable efficiency in addition to the extremely simple synthesis method. Beyond its synthetic simplicity, the procedure employs non-polluting solvents, operates under mild conditions, and generates a highly hydrophobic material. This hydrophobicity is particularly relevant for applications aimed at enhancing the moisture resistance of perovskite-type materials, specifically 3D structures such as $MAPbI_3$.

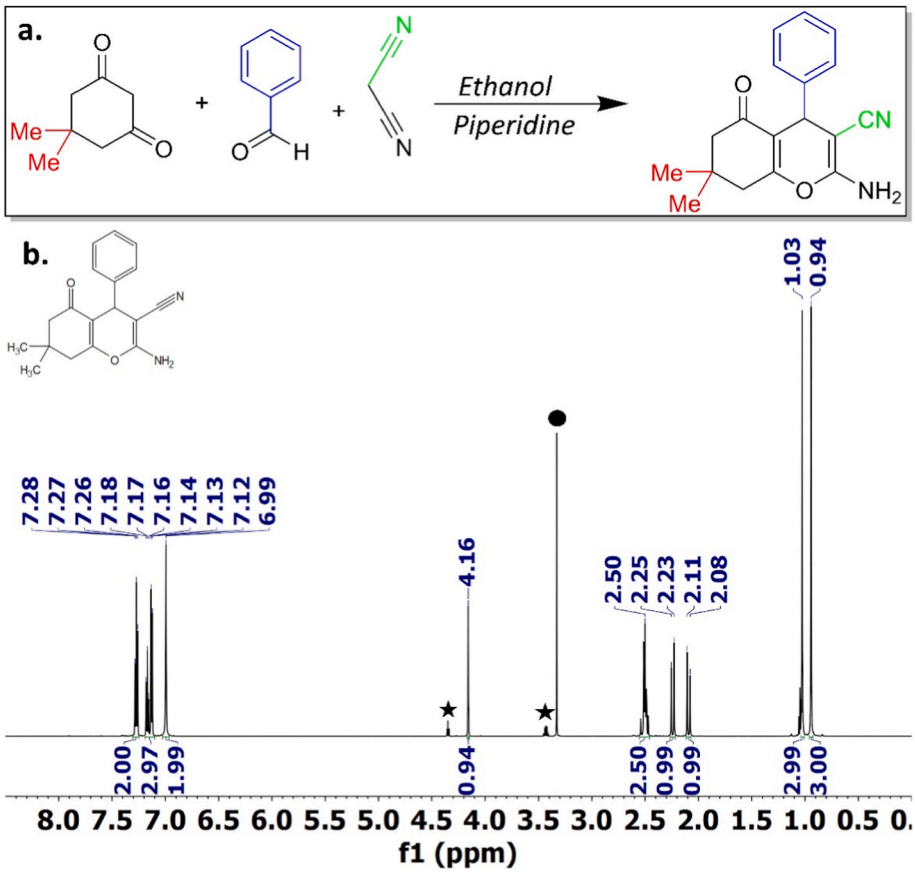

Fig. 1. a. Synthesis of the agent 1. b. ^{1}H NMR spectrum of agent 1 acquired in a 600 MHz spectrophotometer using DMSO-*d6* as solvent. Full circle: residual water. Star, impurities with a concentration lower than 5 %, see discussion in the main text.

Agent 1 was characterized by ^{1}H NMR (Fig. 1b), and comparison with literature data confirmed its high purity [36], eliminating the need for time-consuming purification methods such as chromatography, which typically involve large volumes of hazardous and contaminating solvents. Regarding the two small peaks observed at approximately 4.3 and 3.4 ppm in the ^{1}H NMR spectrum (indicated with a star), these correspond to trace impurities generated during the reaction, most likely as a result of the initial condensation step in the synthetic cycle. These impurities represent approximately 4–5 % relative to the signals of the main compound. We observe that their presence is directly related to the preparation conditions. During the synthesis of agent 1, we used different solvent volumes. We observed that when the reaction mixture was more concentrated (i.e., lower solvent volume), the sudden precipitation of the solid tended to drag along more impurities. In contrast, when the system was more diluted, the resulting solid was significantly purer, although the solvent volume required increased up to threefold. Considering the objectives of our study, we opted for an intermediate concentration that allowed us to obtain a solid with a good level of purity (maximum impurity level around 5 %) without excessive solvent consumption.

Given the diversity of functional groups present in agent 1, which have the potential to passivate defects in hybrid perovskite films, and once its synthesis was completed, its activity as an additive in $MAPI_3$ perovskite films was evaluated. The incorporation in the perovskite films of agent 1 was carried out using two approaches: 1. Addition via the solvent used as an antisolvent (AS), 2. Deposition of a passivating layer of agent 1 (PL). For further details on the experimental procedures, refer to the experimental section. As a first step, thin films were fabricated and characterized by powder X-ray diffraction (pXRD). The initial test involved the preparation of reference $MAPI_3$ thin films and $MAPI_3$ thin films in which agent 1 was included in the antisolvent. All films were stored for approximately 30 days under ambient conditions without any additional precautions. It is important to note that although relative humidity fluctuated throughout the period, it consistently remained at high levels, with an average value of 50 % but with peaks close to 90 %. The formation of $MAPI_3$ was monitored through the characteristic peak at 14.2° of $MAPI_3$, as well as the appearance of PbI_2 at 12.72°, related to the degradation process. Structural characterization via pXRD demonstrated that both methodologies, AS and PL, produced the cubic phase of $MAPI_3$ perovskite consistently, without any detectable additional phases Fig. 2a and b. The emergence of additional phases is probable owing to the incorporation of the agent 1 molecule into the crystal lattice, potentially leading to new diffraction peaks below 10°, analogous to the behavior observed in 2D perovskite systems. However, such features are not observed in the experimental data, suggesting either limited integration of agent 1 into the lattice or a different structural accommodation mechanism that does not produce low-angle reflections. After storing the samples under ambient conditions, X-ray diffraction (XRD) patterns were reacquired to evaluate their structural stability. Degradation was assessed by analyzing the relative intensity of the characteristic peaks: 14.18°, corresponding to the perovskite phase ($MAPI_3$), and 12.72°, associated with PbI_2, a degradation product. In the first experiment, reference films were compared with those treated using agent 1 incorporated into the antisolvent. The results showed significantly greater degradation in the reference films, with the PbI_2 peak accounting for approximately 61 % of the intensity, while the $MAPI_3$ peak represented only 39 %. In contrast, the films treated with agent 1 exhibited markedly improved stability: the PbI_2 peak was ~24 %, and the $MAPI_3$ peak reached ~76 %. This difference suggests that the addition of agent 1 in the antisolvent effectively enhances the film's resistance to moisture. Using the $MAPI_3/PbI_2$ intensity ratio as a stability metric, a fivefold improvement was observed compared to the reference films. In a second experiment, thin films of $MAPI_3$ were fabricated both as reference samples and with agent 1 applied as a passivating layer. As in the previous test, the films were stored for ~30 days under ambient conditions without additional protection. The results were even more outstanding: the reference films showed near-complete degradation, with the PbI_2 peak accounting for ~97 % while that the $MAPI_3$ diffraction peak shows only ~3 % of intensity. Meanwhile, the films with the passivating layer of agent 1 retained much of their original composition, with the PbI_2 peak at ~33 % and the $MAPI_3$ peak at ~67 %, confirming the stabilizing effect of agent 1 under harsh environmental conditions.

These results further demonstrate that the addition of a passivating layer of agent 1 leads to a significant enhancement in the moisture stability of $MAPI_3$ films. Once again, when using the $MAPI_3/PbI_2$ peak intensity ratio as a metric for evaluating stability, a remarkable improvement of approximately 66-fold is observed compared to the reference films.

This result is strongly supported by chemical reasoning. As described in the synthesis section, the synthesized 4HC molecule exhibits high hydrophobicity, which can be inferred from the large number of nonpolar covalent bonds among its constituent atoms. This property provides a crucial advantage, especially considering that many passivating agents, although effective in improving short-term stability and performance, tend to degrade over time due to their chemical nature. Molecules containing a significant proportion of polar covalent bonds (e.g., OH, NH, SH, CO), which often constitute the functional groups responsible for passivation, are prone to interact with ambient moisture, ultimately compromising long-term stability [37].

To further assess the effectiveness of agent 1 in improving stability under operational conditions, complete photovoltaic devices were fabricated. Two key aspects were evaluated: shelf stability (SS) and stabilized power conversion efficiency under maximum power point

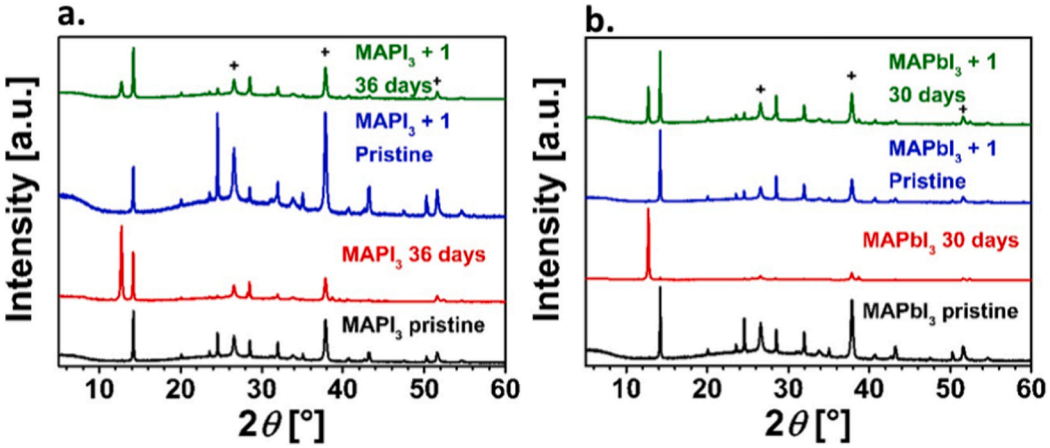

Fig. 2. a. pXRD characterization, via antisolvent method and b. passivating layer.

tracking (MPPT). The corresponding photovoltaic parameters are summarized in Table 1.

Regarding shelf stability, the reference device (without agent 1) exhibited a consistent decline in PCE, dropping to 41 % of its initial value after 170 h of exposure to ambient air (RH = 40 %). In contrast, the device incorporating agent 1 via the antisolvent method showed a significantly smaller reduction of only 13 %, indicating that the reference degraded approximately three times faster. When agent 1 was applied as a passivating layer, degradation was also mitigated, with a PCE drop of 29 %, suggesting a 1.4-fold improvement in stability compared to the reference.

These findings underscore the dual role of agent 1 in enhancing both the intrinsic stability of the perovskite material and the overall performance of the photovoltaic device. The comparative degradation trends are illustrated in Fig. 3. The results showed that passivated solar cells exhibited slightly more stable open-circuit voltage (Voc) values over the course of the study compared to unpassivated devices. Interestingly, and in agreement with the pXRD observations, both the short-circuit current density (Jsc) and the fill factor (FF) demonstrated substantially better performance in the devices passivated with agent 1 than in the reference device.

Given that the pXRD patterns revealed perovskite degradation and the formation of PbI_2, the decrease in Jsc values is likely associated with reduced charge carrier generation due to less efficient light absorption across the electromagnetic spectrum. When comparing the PCE performance curve with those of the other three parameters, it becomes evident that the drop in efficiency most closely mirrors the trend observed in the fill factor curve. This observation suggests that the dominant factor contributing to the decline in PCE may be poor interfacial contact between layers, as an evident consequence of the degradation of the active layer [38].

Maximum power point tracking (MPPT) was performed under continuous 1 sun illumination for 3600 s (Fig. 4). Devices incorporating agent 1 via the antisolvent (AS) method retained 78 % of their initial power conversion efficiency (PCE), while the unpassivated device maintained 74 %. Notably, the PSC with agent 1 applied as a passivating layer preserved 91 % of its original PCE, demonstrating superior operational stability. A detailed analysis of the photovoltaic parameters revealed that the passivated film with the additional layer exhibited enhanced stability, with Voc, Jsc, and FF values retained at 97 %, 94 %, and 98 % of their initial values, respectively. In comparison, the unpassivated film showed retention values of 96 % for Voc, 83 % for Jsc, and 89 % for FF. As in previous observations, the decline in PCE appears to be linked to the degradation pathway from $MAPI_3$ to PbI_2 and the resulting decrease in light-harvesting efficiency, which is consistent with the pXRD findings. In other words, the inclusion of agent 1 not only improves the intrinsic stability of the perovskite film but also enhances the overall device stability under operational conditions—despite the structural simplicity of the molecule.

In most studies available in the literature regarding the use of passivating agents in perovskite films, there is a systematic absence of specific evaluations concerning the intrinsic stability of the substances employed. From our perspective, this represents a critical limitation that must be addressed. It is essential to characterize the chemical and structural behavior of passivating agents under relevant environmental conditions, particularly in the presence of moisture and elevated temperatures, in order to ensure their reliable and long-term application in photovoltaic devices.

Table 1
a. PCE of device without (w/o) agent 1, with (w) agent 1 as antisolvent and passivating layer.

$MAPbI_3$			
J_{sc} (mA●cm^{-2})	V_{oc} (V)	FF (%)	PCE (%)
19.82662	1.03346	77.06919	15.79142
$MAPbI_3$ with Agent 1 as Antisolvent			
J_{sc} (mA●cm^{-2})	V_{oc} (V)	FF (%)	PCE (%)
19.49022	1.00659	74.1668	14.55056
$MAPbI_3$ with Agent 1 as Passivating Layer			
J_{sc} (mA●cm^{-2})	V_{oc} (V)	FF (%)	PCE (%)
21.71906	1.0142	76.32948	16.81345

For this reason, after confirming the beneficial effect of agent 1 on the stability of both the films and the fabricated devices, we focused on evaluating its intrinsic stability. Considering that photovoltaic devices can reach operating temperatures of approximately 85 °C, we conducted a thermal stability study using thermogravimetric analysis (TGA). A slight and consistent mass loss (~1.5 %) was observed between room temperature and 220 °C, likely due to the evaporation of residual solvent. Up to 100 °C, the typical temperature reached during device operation, the mass loss remained minimal, below 0.3 %. On the other hand, given the prolonged exposure of solar cells to elevated temperatures, we further examined long-term stability by conducting an isothermal test at 95 °C for 24 h (Fig. 5a).

The results indicated no significant mass loss, even when measurements were conducted in the presence of air. To determine whether extended thermal exposure altered the chemical composition of agent 1, we acquired its corresponding ^{1}H NMR spectrum. The spectra remained identical to the spectrum of the pristine material, confirming that agent 1 exhibits remarkable thermal stability, Fig. 5b. Although numerous additives have been successfully employed to enhance device efficiency, and to a lesser extent, stability, many of them are liquid in nature. This physical state makes them susceptible to gradual evaporation under sustained thermal stress, potentially initiating device degradation [26, 39,40].

Finally, in line with the goal of developing materials that are both easily synthesizable and industrially accessible, we acquired the ^{1}H NMR spectrum of agent 1 after one year of storage under ambient conditions. The results, once again, confirmed the preservation of its chemical integrity, Fig. 5b. Therefore, we conclude that among the 4HC derivatives, the 4HC evaluated in this study contributes to improving the stability in perovskite-type films and in photovoltaic devices. We would like to point out again that this is despite agent 1 representing the simplest molecule in this family that we propose in this study. This enhancement, beyond being influenced by the functional groups present, may also be attributed to the high intrinsic stability of the material.

To elucidate the interaction mechanism between Agent 1 and the precursors of $MAPbI_3$, we acquired its ^{1}H nuclear magnetic resonance (NMR) spectra. The magnified region of interest (Fig. S2) reveals that all resonances corresponding to the protons of Agent 1 exhibit upfield chemical shifts, indicating a modification in the local electronic environment upon interaction with the perovskite precursors. The complete spectra are provided in Fig. S1 for reference.

The observed phenomenon indicates a relative reduction in the deshielding of hydrogen nuclei, attributable to changes in intermolecular interactions. Under initial conditions, in the absence of perovskite precursors, the protons of Agent 1 predominantly interact with the oxygen atoms of the DMSO solvent through H···O hydrogen bonding. This interaction is particularly strong, favored by the high electronegativity of oxygen and efficient orbital overlap, leading to pronounced deshielding of the hydrogen nuclei involved. Upon incorporation of the precursors PbI_2 and CH_3NH_3I, the chemical environment undergoes a significant modification: the H···O interaction loses predominance and is replaced by H···I interactions. The latter are intrinsically less effective due to the large disparity in atomic size and lower electronegativity, resulting in a less pronounced deshielding compared to the initial conditions, as previously reported [41–44]. Overall, the upfield chemical shifts observed reflect a reorganization of the electronic environment of Agent 1, modulated by the electronegativity and ionic size of the species present, which directly influence hydrogen-bond strength. This modification in chemical shifts suggests the potential of Agent 1 to interact effectively with perovskite precursors within thin films, particularly with iodide anions.

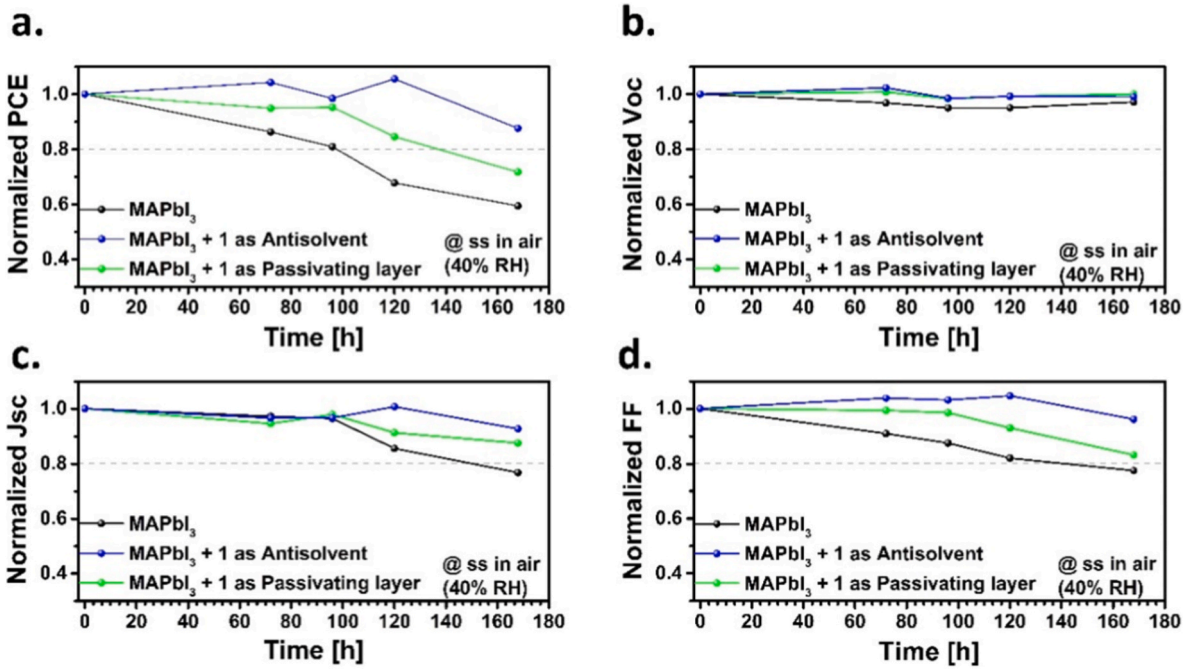

Fig. 3. Performance of the photovoltaic devices in shelf stability, Control (black), antisolvent (blue), passivating layer (green); Normalized PCE (a), Voc (b), Jsc (c) and FF (d).

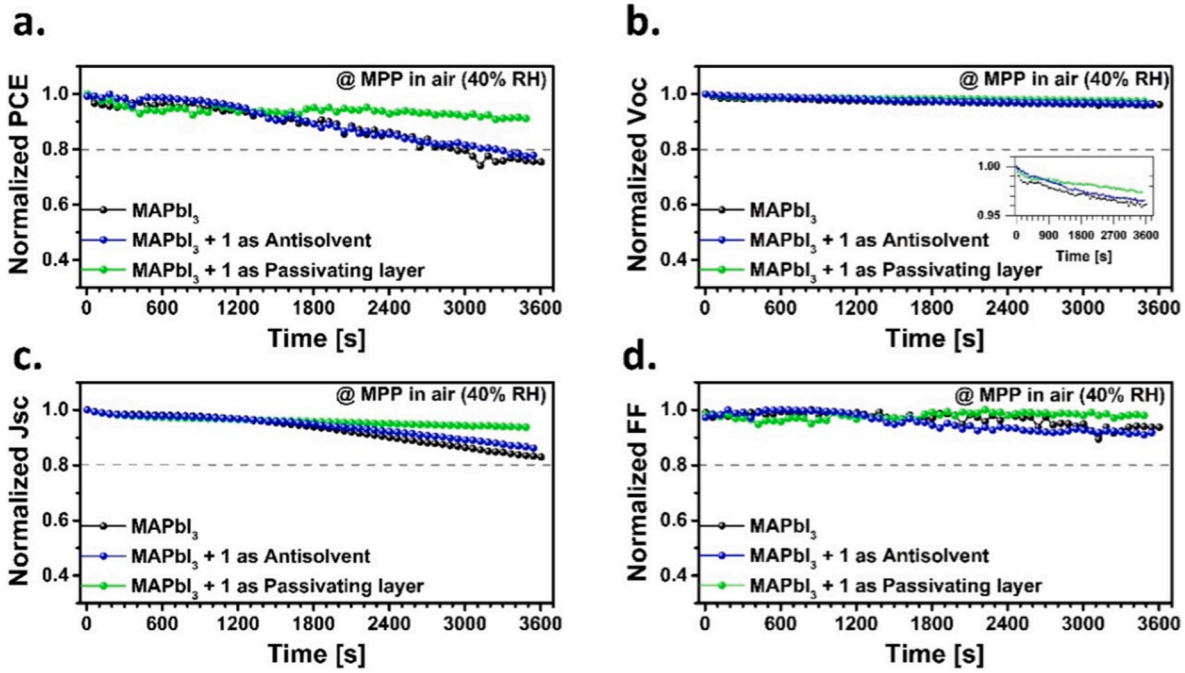

Fig. 4. Performance of the photovoltaic devices in maximum power point tracking, Control (black), antisolvent (blue), passivating layer (green); Normalized PCE (a), Voc (b), Jsc (c) and FF (d).

The presence of multiple Lewis base functional groups (C=O, CN, NH_2) within Agent 1 makes it a strong candidate for iodide vacancy (V_I) passivation through coordination bonds of the type $X \rightarrow M^{2+}$, where X = O or N and M represents a metal ion with an incomplete coordination sphere (Pb^{2+} in this case, but potentially Sn^{2+} as well). To evaluate the feasibility of the $X \rightarrow Pb^{2+}$ interaction, ^{13}C NMR experiments were performed (Fig. S3). This technique is particularly useful to identify coordination of heteroatoms with electron-deficient species, such as incompletely coordinated Pb^{2+}, through chemical shift variations of carbons bound to the involved functional group. Contrary to expectations, carbons bound to oxygen or nitrogen did not exhibit significant shifts. All remaining resonances showed negligible shifts, with some even exhibiting slight upfield shifts; only, as we expect, the carbonyl carbon showed a minor downfield displacement, Fig. S4. Given that DMSO is well known to form stable complexes with Pb^{2+} [45], we hypothesize that the absence of significant shifts arises from competitive solvation, where Agent 1 cannot displace DMSO from the Pb^{2+} coordination sphere.

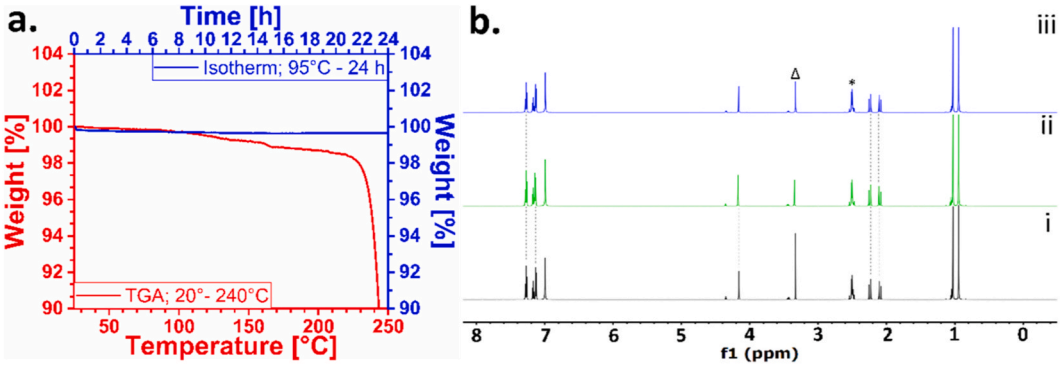

Fig. 5. a. TGA (red) and isothermal analysis (blue) of agent 1. b. ^{1}H NMR of agent 1 fresh (i), ^{1}H NMR of agent 1 after 1 year stored (ii), ^{1}H NMR of agent 1 one year stored + 24 h at 95 °C (iii) (Δ corresponding to water in DMSO-d6, * blue is residual DMSO).

To test this hypothesis, solution FTIR spectra were acquired under four conditions: (i) pure DMSO, (ii) DMSO + PbI_2, (iii) DMSO + PbI_2 + Agent 1, and (iv) DMSO + Agent 1. Considering the structure of DMSO, we focus on the behavior of the S=O group, which will surely serve as a Lewis base coordinating PbI_2 [46]. Concerning the S=O stretching band (1043, 1019 cm^{-1}) of DMSO, its profile showed a clear modification upon interaction with PbI_2. Upon addition of Agent 1 to the DMSO/PbI_2 system, no substantial change was observed in the characteristic band (Fig. S5), indicating that the S=O → Pb^{2+} interactions remained unaffected. Besides, examination of the functional groups of Agent 1 revealed that the vibrational bands associated with -CN (2188 cm^{-1}), C=O (1664 cm^{-1}), and C–N (amine, 1214 cm^{-1}) were unchanged, regardless of the presence or absence of PbI_2. These results demonstrate that, in the presence of DMSO, Agent 1 does not coordinate to the metallic center. This observation is consistent with the ^{13}C NMR data, thereby supporting the hypothesis that Agent 1 does not interact with Pb^{2+} in DMSO solution.

However, given the positive influence of Agent 1 on shelf and operational stability, we hypothesized that coordination must occur in the solid state, specifically in thin films. Films were fabricated by introducing Agent 1 either via antisolvent addition or as a passivation layer. Due to the detection limit of the FTIR setup, the presence of Agent 1 could not be confirmed in the initial experiments. Therefore, the fabrication method was modified by adding 10 mg of Agent 1 directly into the precursor solution. FTIR spectra of the resulting films unequivocally revealed the presence of the expected functional groups: NH_2 (3422 cm^{-1} and 3359 cm^{-1}), -CN (2190 cm^{-1}), C=O (1648 cm^{-1}), Fig. S6. Interestingly, all bands exhibited shifts: hypsochromic for -CN and C=O, and bathochromic for -NH_2. The hypsochromic shifts observed for -CN and C=O may reflect restricted vibrational motion within densely packed films, as previously reported [47,48]. In contrast, the bathochromic shift of the N–H stretching vibration is consistent with bond weakening (elongation), originating from donation of the nitrogen lone pair to a metal center with an incomplete coordination sphere [49,50]. This observation suggests that Agent 1 behaves as a passivator of V_I, where the coordinating agent is the amino group through –NH_2→Pb^{2+} interactions. It has been reported that the presence or generation of V_I triggers the degradation of the perovskite $MAPbI_3$ material through iodide ion (I^-) migration, followed by its oxidation to I_2 [51–54]. To verify this hypothesis, both fresh and aged films were immersed in toluene for 15 min to extract the I_2 formed within the crystal lattice. The resulting solutions were analyzed by absorption spectroscopy, as shown in Fig. S7. The results revealed a higher concentration of I_2 in freshly prepared films compared to those aged 20 days. In fresh films, degradation processes promoted by V_I are only beginning, and the migration/oxidation pathway is strongly favored, resulting in a greater presence of I_2. In contrast, aged films—where the degradation (migration/oxidation) of I^- has been ongoing for several days—exhibited lower levels of extracted I_2, likely due to its prior release into the environment [55]. To evaluate the passivation performance of Agent 1 in the reported conditions, three types of thin films were prepared: (i) unpassivated, (ii) passivated by antisolvent addition, and (iii) passivated by an additional layer containing Agent 1. Spectroscopic analysis after toluene extraction of fresh films revealed clear differences in I_2 concentration, Fig. S8. The highest concentration was detected in unpassivated films, followed by antisolvent-passivated films, while the lowest concentration was observed in films with the additional Agent 1 layer. These results suggest that I_2 release, and thus V_I density, is mitigated by Agent 1. The antisolvent route produced a positive but limited effect, whereas the additional layer provided stronger passivation, likely due to higher local concentration of Agent 1 at the film surface.

This proposed mechanism is consistent with the photovoltaic performance observed in our solar cells: the presence of Agent 1 delays the decline of Jsc and FF, thereby contributing to the structural integrity and operational stability of the devices [54]. Furthermore, the reduced I_2 concentration in passivated films supports the FTIR-derived hypothesis that Agent 1 interacts with Pb^{2+} centers, effectively passivating iodide vacancies and preventing subsequent degradation processes, including I^- migration and oxidation to form I_2.

The comprehensive evaluation of agent 1 across multiple configurations—incorporation via antisolvent and as a passivating layer—consistently demonstrated a significant enhancement in both material and device stability. The minimal degradation observed in shelf-life tests, MPPT, and thermal stability assessments underscores the robustness of agent 1 under operational and environmental stressors.

4. Conclusions

This work introduces agent 1 as a multifunctional organic additive that significantly enhances the environmental and operational stability of $MAPbI_3$ perovskite films. Synthesized via a one-pot reaction in ethanol, agent 1 offers a scalable and green fabrication route, aligning with sustainable manufacturing principles. Its integration through antisolvent treatment and surface passivation reduces moisture-induced degradation and improves long-term device performance. Treated films retained up to 67 % of their structure under high humidity, while solar cells preserved over 90 % of their initial efficiency during continuous operation. Beyond performance, agent 1 exhibits exceptional thermal and chemical resilience, maintaining molecular integrity after prolonged stress and storage. These combined attributes—stability, processability, and environmental safety—position agent 1 as a compelling candidate for industrial-scale stabilization of perovskite solar technologies, advancing the path toward durable and sustainable photovoltaics.

Credit author statement

Miguel Guerrero: Writing – review & editing, Writing – original draft, Methodology, Investigation, Formal analysis, Data curation. **Jesús**

Sanchez-Diaz: Writing – review & editing, Methodology, Investigation, Formal analysis, Data curation. **Gabriela S. Anaya-González:** Investigation. **Oscar González-Antonio:** Investigation. **Lorena Martínez-dlCruz:** Experimental procedures and investigation. **Margarita Romero-Ávila:** Resources. **Rosa Santillan:** Writing – review & editing, Resources. **Iván Mora-Seró:** Writing – review & editing, Supervision, Resources. **Jesús Rodríguez-Romero:** Writing – review & editing, Writing – original draft, Supervision, Resources, Project administration, Funding acquisition, Formal analysis, Data curation, Conceptualization.

Declaration of competing interest

The authors declare that they have no known competing financial interests or personal relationships that could have appeared to influence the work reported in this paper.

Acknowledgments

We thank the projects PAPIIT IA208621, PAIP 5000–9190 for the financial support. M. G. expresses his gratitude to SECIHTI for the graduate scholarship support CVU:1341568. G. S. A. G. would like to CONAHCyT for the postdoctoral fellowship 660915. O. G-A thanks SECIHTI for his postdoctoral fellowship (CVU 289250). We thank Q. Daniel Rangel Partido and Q. Angel de Jesús Ferrer Montiel for valuable scientific discussions. We also acknowledge Maricela Gutiérrez Franco, Nayelli López Balbiaux, and Rafael Iván Puente Lee for their technical assistance.

Appendix A. Supplementary data

Supplementary data to this article can be found online at https://doi.org/10.1016/j.mtener.2026.102197.

Data availability

Data will be made available on request.

References

[1] J. Troughton, K. Hooper, T.M. Watson, Humidity resistant fabrication of CH3NH3PbI3 perovskite solar cells and modules, Nano Energy 39 (2017) 60–68, https://doi.org/10.1016/j.nanoen.2017.06.039.
[2] N. Aristidou, I. Sanchez-Molina, T. Chotchuangchutchaval, M. Brown, L. Martinez, T. Rath, S.A. Haque, The role of oxygen in the degradation of methylammonium lead trihalide perovskite photoactive layers, Angew. Chem. Int. Ed. 54 (2015) 8208–8212, https://doi.org/10.1002/anie.201503153.
[3] K. Choi, J. Lee, H. Choi, G.-W. Kim, H.I. Kim, T. Park, Heat dissipation effects on the stability of planar perovskite solar cells, Energy Environ. Sci. 13 (2020) 5059–5067, https://doi.org/10.1039/D0EE02859B.
[4] T. Wu, X. Li, Y. Qi, Y. Zhang, L. Han, Defect passivation for perovskite solar cells: from molecule design to device performance, ChemSusChem 14 (2021) 4354–4376, https://doi.org/10.1002/cssc.202101573.
[5] Y. Wu, F. Xie, H. Chen, X. Yang, H. Su, M. Cai, Z. Zhou, T. Noda, L. Han, Thermally stable $MAPbI_3$ Perovskite Solar Cells with Efficiency of 19.19% and Area over 1 cm^2 achieved by Additive Engineering, Adv. Mater. 29 (2017) 1701073, https://doi.org/10.1002/adma.201701073.
[6] J. Luo, J. Xia, H. Yang, H.A. Malik, F. Han, H. Shu, X. Yao, Z. Wan, C. Jia, Novel approach toward hole-transporting layer doped by hydrophobic Lewis acid through infiltrated diffusion doping for perovskite solar cells, Nano Energy 70 (2020) 104509, https://doi.org/10.1016/j.nanoen.2020.104509.
[7] X. Li, W. Sheng, X. Duan, Z. Lin, J. Yang, L. Tan, Y. Chen, Defect passivation effect of chemical groups on perovskite solar cells, ACS Appl. Mater. Interfaces 14 (2022) 34161–34170, https://doi.org/10.1021/acsami.1c08539.
[8] M.A.R. Laskar, W. Luo, N. Ghimire, A.H. Chowdhury, B. Bahrami, A. Gurung, K. M. Reza, R. Pathak, R.S. Bobba, B.S. Lamsal, K. Chen, M.T. Rahman, S.I. Rahman, K. Emshadi, T. Xu, M. Liang, W.H. Zhang, Q. Qiao, Phenylhydrazinium iodide for surface passivation and defects suppression in perovskite solar cells, Adv. Funct. Mater. 30 (2020) 2000778, https://doi.org/10.1002/adfm.202000778.
[9] Z. Yang, J. Dou, S. Kou, J. Dang, Y. Ji, G. Yang, W.Q. Wu, D.B. Kuang, M. Wang, Multifunctional phosphorus-containing lewis acid and base passivation enabling efficient and moisture-stable perovskite solar cells, Adv. Funct. Mater. 30 (2020) 1910710, https://doi.org/10.1002/adfm.201910710.
[10] C. Shen, T. Ye, P. Yang, G. Chen, All–Inorganic perovskite solar cells: defect regulation and emerging applications in extreme environments, Adv. Mater. 36 (2024) 2401498, https://doi.org/10.1002/adma.202401498.
[11] E.J. Juarez-Perez, L.K. Ono, M. Maeda, Y. Jiang, Z. Hawash, Y. Qi, Photodecomposition and thermal decomposition in methylammonium halide lead perovskites and inferred design principles to increase photovoltaic device stability, J. Mater. Chem. A 6 (2018) 9604–9612, https://doi.org/10.1039/C8TA03501F.
[12] K. Wang, J. Liu, J. Yin, E. Aydin, G.T. Harrison, W. Liu, S. Chen, O.F. Mohammed, S. De Wolf, Defect passivation in perovskite solar cells by cyano-based π-Conjugated molecules for improved performance and stability, Adv. Funct. Mater. 30 (2020) 2002861, https://doi.org/10.1002/adfm.202002861.
[13] F. Li, J. Yuan, X. Ling, Y. Zhang, Y. Yang, S.H. Cheung, C.H.Y. Ho, X. Gao, W. Ma, A universal strategy to utilize polymeric semiconductors for perovskite solar cells with enhanced efficiency and longevity, Adv. Funct. Mater. 28 (2018) 1706377, https://doi.org/10.1002/adfm.201706377.
[14] L. Zuo, H. Guo, D.W. deQuilettes, S. Jariwala, N. De Marco, S. Dong, R. DeBlock, D. S. Ginger, B. Dunn, M. Wang, Y. Yang, Polymer-modified halide perovskite films for efficient and stable planar heterojunction solar cells, Sci. Adv. 3 e1700106, DOI: https://doi.org/10.1126/sciadv.1700106.
[15] Y. Yang, L. Wu, X. Hao, Z. Tang, H. Lai, J. Zhang, W. Wang, L. Feng, Beneficial effects of potassium iodide incorporation on grain boundaries and interfaces of perovskite solar cells, RSC Adv. 9 (2019) 28561–28568, https://doi.org/10.1039/C9RA05371A.
[16] J. Xie, K. Yan, H. Zhu, G. Li, H. Wang, H. Zhu, P. Hang, S. Zhao, W. Guo, D. Ye, L. Shao, X. Guan, T. Ngai, X. Yu, J. Xu, Identifying the functional groups effect on passivating perovskite solar cells, Sci. Bull. 65 (2020) 1726–1734, https://doi.org/10.1016/j.scib.2020.05.031.
[17] W. Yan, W. Yang, K. Zhang, H. Yu, Y. Yang, H. Fan, Y. Qi, H. Xin, Enhancing performance and stability of perovskite solar cells through surface defect passivation with organic bidentate lewis bases, ACS Omega 7 (2022) 32383–32392, https://doi.org/10.1021/acsomega.2c03802.
[18] S.-P. Cho, H.-J. Lee, Y.-H. Seo, S.-I. Na, Multifunctional passivation agents for improving efficiency and stability of perovskite solar cells: synergy of methyl and carbonyl groups, Appl. Surf. Sci. 575 (2022) 151740, https://doi.org/10.1016/j.apsusc.2021.151740.
[19] J. Tan, R. Tang, R. Wang, X. Gao, K. Chen, X. Liu, F. Wu, L. Zhu, Thiocarbonyl-Based hole transport materials with enhanced defect passivation ability for efficient and stable perovskite solar cells, Small 20 (2024) 2402760, https://doi.org/10.1002/smll.202402760.
[20] S. Shahbazi, M.-Y. Li, A. Fathi, E.W.-G. Diau, Realizing a cosolvent System for stable tin-based perovskite solar cells using a two-step deposition approach, ACS Energy Lett. 5 (2020) 2508–2511, https://doi.org/10.1021/acsenergylett.0c01190.
[21] Z. Feng, Z. Xia, Z. Wu, Y. Hua, G. Zhu, X. Chen, S. Huang, Efficient and stable perovskite solar cells via organic surfactant interfacial passivation, Sol. Energy 227 (2021) 438–446, https://doi.org/10.1016/j.solener.2021.09.032.
[22] D. Song, D. Wei, P. Cui, M. Li, Z. Duan, T. Wang, J. Ji, Y. Li, J.M. Mbengue, Y. Li, Y. He, M. Trevor, N.-G. Park, Dual function interfacial layer for highly efficient and stable lead halide perovskite solar cells, J. Mater. Chem. A 4 (2016) 6091–6097, https://doi.org/10.1039/C6TA00577B.
[23] J. Wu, M. Hu, L. zhang, G. Song, Y. Li, W. Tan, Y. Tian, B. Xu, Fluorinated cross-linkable and Dopant-free hole transporting materials for efficient and stable perovskite solar cells, Chem. Eng. J. 422 (2021) 130124, https://doi.org/10.1016/j.cej.2021.130124.
[24] N. Cai, F. Li, Y. Chen, R. Luo, T. Hu, F. Lin, S.-M. Yiu, D. Liu, D. Lei, Z. Zhu, A.K. Y. Jen, Synergistical dipole–dipole interaction induced self-assembly of phenoxazine-based hole-transporting materials for efficient and stable inverted perovskite solar cells, Angew. Chem. Int. Ed. 60 (2021) 20437–20442, https://doi.org/10.1002/anie.202107020.
[25] A. Abate, M. Saliba, D.J. Hollman, S.D. Stranks, K. Wojciechowski, R. Avolio, G. Grancini, A. Petrozza, H.J. Snaith, Supramolecular halogen bond passivation of organic–inorganic halide perovskite solar cells, Nano Lett. 14 (2014) 3247–3254, https://doi.org/10.1021/nl500627x.
[26] N.K. Noel, A. Abate, S.D. Stranks, E.S. Parrott, V.M. Burlakov, A. Goriely, H. J. Snaith, Enhanced photoluminescence and solar cell performance *via* Lewis base passivation of organic–inorganic lead halide perovskites, ACS Nano 8 (2014) 9815–9821, https://doi.org/10.1021/nn5036476.
[27] X. Wu, J. Deng, T. Yang, L. Fu, J. Xu, Small molecule induced interfacial defect healing to construct inverted perovskite solar cells with high fill factor and stability, J. Colloid Interface Sci. 678 (2025) 776–784, https://doi.org/10.1016/j.jcis.2024.08.186.
[28] H. Na, M. Qiang Li, J. Cha, S. Kim, H. Jin, D. Baek, M. Kyong Kim, S. Sim, M. Lee, M. Kim, J. Lim, J. Lee, M. Kim, Passivating detrimental grain boundaries in perovskite films with strongly interacting polymer for achieving high-efficiency and stable perovskite solar cells, Appl. Surf. Sci. 626 (2023) 157209, https://doi.org/10.1016/j.apsusc.2023.157209.
[29] K.B. Ramesh, A.S. Manjunatha, M. Srinivas, M.A. Pasha, Eco-friendly synthesis of indole-4-hydroxy-chromen-2-ones using green zinc oxide nanocatalyst and its assessment of anti-cancer studies against A549 cells, Inorg. Chem. Commun. 169 (2024) 113012, https://doi.org/10.1016/j.inoche.2024.113012.
[30] A. Feliciano, O. Gómez-García, C.H. Escalante, M.A. Rodríguez-Hernández, M. Vargas-Fuentes, D. Andrade-Pavón, L. Villa-Tanaca, C. Álvarez-Toledano, M. T. Ramírez-Apan, M.A. Vázquez, J. Tamariz, F. Delgado, Three-Component synthesis of 2-Amino-3-cyano-4H-chromenes, in Silico analysis of their pharmacological profile, and in vitro anticancer and antifungal testing, Pharmaceuticals 14 (2021), https://doi.org/10.3390/ph14111110.

[31] K.N. Sharon, P. Padmaja, P.N. Reddy, A brief review on the synthesis of 4H-Chromene-Embedded heterocycles, ChemistrySelect 9 (2024) e202400565, https://doi.org/10.1002/slct.202400565.
[32] S. Rostamnia, A. Nuri, H. Xin, A. Pourjavadi, S.H. Hosseini, Water dispersed magnetic nanoparticles (H2O-DMNPs) of γ-Fe2O3 for multicomponent coupling reactions: a green, single-pot technique for the synthesis of tetrahydro-4H-chromenes and hexahydroquinoline carboxylates, Tetrahedron Lett. 54 (2013) 3344–3347, https://doi.org/10.1016/j.tetlet.2013.04.048.
[33] N.G. Khaligh, T. Mihankhah, M.R. Johan, Synthesis of new low-viscous sulfonic acid-functionalized ionic liquid and its application as a Brönsted liquid acid catalyst for the one-pot mechanosynthesis of 4H-pyrans through the ball milling process, J. Mol. Liq. 277 (2019) 794–804, https://doi.org/10.1016/j.molliq.2019.01.024.
[34] S. Wada, H. Suzuki, Calcite and fluorite as catalyst for the Knövenagel condensation of malononitrile and methyl cyanoacetate under solvent-free conditions, Tetrahedron Lett. 44 (2003) 399–401, https://doi.org/10.1016/S0040-4039(02)02431-0.
[35] C. Wiles, P. Watts, S.J. Haswell, E. Pombo-Villar, The preparation and reaction of enolates within micro reactors, Tetrahedron 61 (2005) 10757–10773, https://doi.org/10.1016/j.tet.2005.08.076.
[36] M.R. Maurya, N. Kumar, F. Avecilla, Controlled modification of Triaminoguanidine-Based μ3 ligands in multinuclear [VIVO]/[VVO2] complexes and their catalytic potential in the synthesis of 2-Amino-3-cyano-4H-pyrans/4H-chromenes, Inorg. Chem. 63 (2024) 2505–2524, https://doi.org/10.1021/acs.inorgchem.3c03704.
[37] M. Azam, Y. Ma, B. Zhang, X. Shao, Z. Wan, H. Zeng, H. Yin, J. Luo, C. Jia, Tailoring pyridine bridged chalcogen-concave molecules for defects passivation enables efficient and stable perovskite solar cells, Nat. Commun. 16 (2025) 602, https://doi.org/10.1038/s41467-025-55815-z.
[38] W. Nie, H. Tsai, R. Asadpour, J.-C. Blancon, A.J. Neukirch, G. Gupta, J.J. Crochet, M. Chhowalla, S. Tretiak, M.A. Alam, H.-L. Wang, A.D. Mohite, High-efficiency solution-processed perovskite solar cells with millimeter-scale grains, Science 347 (2015) 522–525, https://doi.org/10.1126/science.aaa0472.
[39] Y.-H. Seo, E.-C. Kim, S.-P. Cho, S.-S. Kim, S.-I. Na, High-performance planar perovskite solar cells: influence of solvent upon performance, Appl. Mater. Today 9 (2017) 598–604, https://doi.org/10.1016/j.apmt.2017.11.003.
[40] J. Li, X. Hua, F. Gao, X. Ren, C. Zhang, Y. Han, Y. Li, B. Shi, S. Liu, Green antisolvent additive engineering to improve the performance of perovskite solar cells, J. Energy Chem. 66 (2022) 1–8, https://doi.org/10.1016/j.jechem.2021.06.023.
[41] A. Semerci, J. Urieta-Mora, S. Driessen, A. Buyruk, R. Hooijer, A. Molina-Ontoria, B. Alkan, S. Akin, M. Fanetti, H. Balakrishnan, A. Hartschuh, S. Tao, N. Martín, P. Müller-Buschbaum, S. Emin, T. Ameri, The role of fluorine-functionalized organic spacers for defect passivation and low-dimensional phase Formation in 3D MAPI perovskite solar cells, Adv. Funct. Mater. 35 (2025) 2423109, https://doi.org/10.1002/adfm.202423109.
[42] S. Galve-Lahoz, J. Sánchez-Diaz, C. Echeverría-Arrondo, J. Simancas, J. Rodriguez-Pereira, S.-H. Turren-Cruz, J.P. Martinez-Pastor, I. Mora-Seró, J.L. Delgado, Addressing ambient stability challenges in pure FASnI3 perovskite solar cells through organic additive engineering, J. Mater. Chem. A 12 (2024) 21933–21943, https://doi.org/10.1039/D4TA03291H.
[43] T. Liu, J. Guo, D. Lu, Z. Xu, Q. Fu, N. Zheng, Z. Xie, X. Wan, X. Zhang, Y. Liu, Y. Chen, Spacer engineering using aromatic formamidinium in 2D/3D hybrid perovskites for highly efficient solar cells, ACS Nano 15 (2021) 7811–7820, https://doi.org/10.1021/acsnano.1c02191.
[44] X. Li, M. Ibrahim Dar, C. Yi, J. Luo, M. Tschumi, S.M. Zakeeruddin, M. K. Nazeeruddin, H. Han, M. Grätzel, Improved performance and stability of perovskite solar cells by crystal crosslinking with alkylphosphonic acid ω-ammonium chlorides, Nat. Chem. 7 (2015) 703–711, https://doi.org/10.1038/nchem.2324.
[45] J. Selbin, W.E. Bull, L.H. Holmes, Metallic complexes of dimethylsulphoxide, J. Inorg. Nucl. Chem. 16 (1961) 219–224, https://doi.org/10.1016/0022-1902(61)80493-4.
[46] R.S. Drago, The infrared spectra of some dimethyl sulfoxide complexes, in: D. Meek (Ed.), J. Phys. Chem. (1961) 1446–1447, https://doi.org/10.1021/j100826a505.
[47] J. Li, F. Gao, J. Wen, Z. Xu, C. Zhang, X. Hua, X. Cai, Y. Li, B. Shi, Y. Han, X. Ren, S. Liu, Effective surface passivation with 4-bromo-benzonitrile to enhance the performance of perovskite solar cells, J. Mater. Chem. C 9 (2021) 17089–17098, https://doi.org/10.1039/D1TC04615B.
[48] B. Shi, Y. Li, F. Gao, J. Li, X. Cai, C. Zhang, Y. Wu, C. Lu, J. Wang, S. Liu, Enhancing the performance of perovskite solar cells by 4-Chloro-1,8-Naphthalic anhydride for surface passivation, Adv. Mater. Interfaces 10 (2023) 2201809, https://doi.org/10.1002/admi.202201809.
[49] K. Zou, Q. Li, J. Fan, H. Tang, L. Chen, S. Tao, T. Xu, W. Huang, Pyridine derivatives' surface passivation enables efficient and stable carbon-based perovskite solar cells, ACS Mater. Lett. 4 (2022) 1101–1111, https://doi.org/10.1021/acsmaterialslett.2c00123.
[50] D. Lu, J. Fan, X. Ma, M. Geng, J. Li, T. Xu, Dual-Functional passivation agent of natural dye Congo red for enhanced carbon-based perovskite solar cells, ACS Appl. Mater. Interfaces 16 (2024) 69439–69449, https://doi.org/10.1021/acsami.4c16831.
[51] J. Schoonman, Organic–inorganic lead halide perovskite solar cell materials: a possible stability problem, Chem. Phys. Lett. 619 (2015) 193–195, https://doi.org/10.1016/j.cplett.2014.11.063.
[52] A. Kaldor, G.A. Somorjai, Photodecomposition of Lead Chloride, J. Phys. Chem. 70 (1966) 3538–3544, https://doi.org/10.1021/j100883a030.
[53] S. Kundu, T.L. Kelly, In situ studies of the degradation mechanisms of perovskite solar cells, EcoMat 2 (2020) e12025, https://doi.org/10.1002/eom2.12025.
[54] N. Aristidou, C. Eames, I. Sanchez-Molina, X. Bu, J. Kosco, M.S. Islam, S.A. Haque, Fast oxygen diffusion and iodide defects mediate oxygen-induced degradation of perovskite solar cells, Nat. Commun. 8 (2017) 15218, https://doi.org/10.1038/ncomms15218.
[55] C. Gong, H. Zhang, Q. Lu, W. Huang, R. Chen, L. Xu, Dual-site vacancy filling strategy enhances efficiency and stability of tin-based perovskite solar cells, J. Colloid Interface Sci. 701 (2026) 138641, https://doi.org/10.1016/j.jcis.2025.138641.